

# A Reduced-Order Simulated Annealing Approach for Four-Dimensional Variational Data Assimilation in Meteorology and Oceanography

I. Hoteit\*

*Scripps Institution of Oceanography*

*La Jolla, CA, 92093, USA*

## SUMMARY

Four-dimensional variational data assimilation in meteorology and oceanography suffers from the presence of local minima in the cost function. These local minima arise when the system under study is strongly nonlinear. The number of local minima further dramatically increases with the length of the assimilation period, and often renders the solution of the problem intractable. Global optimization methods are therefore needed to resolve this problem. However, the huge computational burden makes the application of these sophisticated techniques unfeasible for large variational data assimilation systems. In this study, a Simulated Annealing (SA) algorithm, complemented with an order-reduction of the control vector, is used to tackle this problem. SA is a very powerful tool of combinatorial minimization in the presence of several local minima at the cost of increasing the execution time. Order-reduction is then used to reduce the dimension of the search space in order to speed up the

---

\*Correspondence to: I. Hoteit, Scripps Institution of Oceanography, Physical Oceanography Research Division, Nierenburg Hall, 9500 Gilman Drive, La Jolla, California 92093-0230, U.S.A.; Email: [ihoteit@ucsd.edu](mailto:ihoteit@ucsd.edu)

Contract/grant sponsor: Publishing Arts Research Council; contract/grant number: 98–1846389

*Received 19 February 2007*

*Revised ?? September 2007*

convergence rate of the SA algorithm. This is achieved through a proper orthogonal decomposition (POD). The new approach was implemented with a realistic eddy-permitting configuration of the Massachusetts Institute of Technology general circulation model (MITgcm) of the tropical Pacific Ocean. Numerical results indicate that the reduced-order simulated annealing approach was able to efficiently reduce the cost function with a reasonable number of function evaluations.

Copyright © 2000 John Wiley & Sons, Ltd.

KEY WORDS: Data assimilation, 4D-VAR, Simulated Annealing, Order Reduction, Tropical Pacific

## 1. INTRODUCTION

Four dimensional variational data assimilation (4D-VAR) is widely used in meteorology and oceanography for estimating the model state and poorly known parameters [11, 47]. It is equivalent to the fixed-interval smoothing problem in the control literature. The basic idea of this approach is to find the model trajectory that best fits available observations over a given period of time, while adjusting a well-chosen set of uncertain model parameters, called control variables. A cost function  $\mathbf{J}$ , measuring the discrepancy between the observations and their counterparts described by a numerical model, is first defined. The 4D-VAR problem then seeks for the minimum of  $\mathbf{J}$  with respect to the control variables, while the dynamics describing the temporal evolution of the model state variables act as a set of strong constraints, i.e. they are fulfilled exactly. Optimization methods are then used to minimize the cost function  $\mathbf{J}$  with respect to the chosen set of control variables.

Because of the complexity of the 4D-VAR problem in meteorology and oceanography, the variational equations are solved implicitly and iteratively in practice, employing the gradients of the cost function and an optimization algorithm [47]. The adjoint method is computationally the most efficient method to determine the gradients - this is known as reverse-mode differentiation [22]. It provides this information at the cost of a few model integrations, while integrating the adjoint of the tangent linear model backward in time [22]. The optimization is then carried out using gradient-based descent algorithms, such as ‘quasi-Newton’ or ‘conjugate gradient’, which are characterized by fast convergence rates at the risk of converging toward the closest local minima [47].

The use of the adjoint method for data assimilation with nonlinear models can be problematic. When the model is sufficiently nonlinear, the cost function becomes non-convex, implying the existence of multiple local minima [26, 35]. This may prevent significant

reduction in the cost function when using a gradient descent optimization algorithm, as these algorithms are only designed to converge toward local minima. Recently, several studies reported exponentially growing sensitivities in the adjoint model (e.g. [15, 19, 21, 49]). These small-scale but strong gradients indicate the presence of many small-amplitude but tightly packed extrema [19]. Sensitivities grow exponentially large in the adjoint model because the linearized model lacks the nonlinear interactions that otherwise slow or stop the exponential growth once the perturbations reach finite amplitude [49]. These strong linear sensitivities, which have been associated with rapidly-growing perturbations (“intrinsic variability”) that are not easily predictable or controllable by the system, invalidate the use of the gradient for descent [15, 19]. Of course, one can always apply the 4DVAR assimilation over short periods in which the linear approximation holds. However, this would only hide the problem, but do not address it. Splitting the assimilation window into small periods means less information from the observation to estimate the poorly observed state of the ocean and the atmosphere. This would also lead to dynamically discontinuous state estimates with initial conditions not consistent with the state estimate at the end of the previous assimilation window. These issues are even more pronounced with strongly nonlinear high resolution models where the adjoint gradients can only be useful over very short periods where the linear approximation holds.

Several approaches have been proposed to extend the limits of the adjoint method in the presence of strong nonlinearities by basically replacing the original unstable adjoint model with the adjoint of a tangent linear model which has been modified to be stable. This involves a simplification of the original tangent linear model and is usually obtained by omitting strongly unstable modes [15, 19, 49]. The gradients calculated by the modified adjoint do not “see” the secondary minima and approximate the full gradients to the envelope of the cost function. The omission of strongly nonlinear variations in the adjoint model inevitably leads to loss of

accuracy in the 4D-VAR solution. In this study we will resort to a different approach to tackle a strongly nonlinear 4D-VAR problem by employing a global optimization technique, namely a Simulated Annealing (SA) algorithm. SA is a very powerful tool of combinatorial minimization in the presence of several local minima [18]. Its concept is based on the manner in which a metal is ‘annealed’ in order to increase its strength; when a metal is cooled slowly, it freezes into the minimum-energy crystalline structure. This optimization technique is generally quite easy to implement and, more importantly, does not require the development of an adjoint model. Specifically, an SA algorithm searches about randomly in the control space looking for the solution that minimizes the value of a cost function. Thus, only evaluations of the cost function are required for the algorithm. Because of its stochastic nature, a SA algorithm is independent of the analytical properties of the cost function and of the start point of the optimization, unlike gradient-based optimization techniques. Several studies successfully resorted to SA to solve different low-dimensional nonlinear 4D-VAR problems. Examples of applications of SA to 4D-VAR problems in physical oceanography are [1, 20], in marine ecosystems [16, 27, 44], and in hydrology [33].

The convergence rate of an SA algorithm is largely determined by the parameters of the “annealing process” [37]. In this study, an SA algorithm developed by [12], which employs an efficient method to explore the solution space, was adopted. This algorithm was shown to be quite performant with mid-size optimization problems [12]. The portability of this algorithm to realistic 4D-VAR oceanic and atmospheric problems is not feasible, however, because of the huge dimension of the control vector usually considered in these systems, typically of the order of  $10^7 - 10^8$ . Giving that only few (tens to hundreds) cost function evaluations are allowed in such systems, as the numerical integration of realistic oceanic and atmospheric numerical models can be quite expensive, a drastic reduction of the dimension of the search space is

unavoidable.

One way to improve the convergence rate of an optimization is to carry it in a smaller dimensional subspace. This is the idea behind the linearly-equivalent dual formulation (also called the Physical-space Statistical Analysis System (PSAS)<sup>†</sup>) of the variational adjoint approach [7], which consists of performing searches for the optimum solution in the data space rather than the large control space. However, given the large - and ever increasing - number of observations now available, the benefits of the dual approach are becoming rather limited. Another way to reduce the dimensions of the line search is to project the control vector onto a subspace of much smaller dimensions through an order-reduction. Off course, this entails an approximation which generally reduces the performance of the optimization because of the restricted number of allowed line search directions. However, as argued by several authors [3, 5, 8, 14, 39, 45] who applied order-reduction to speed-up the convergence rate of adjoint-based 4D-VAR problems, this loss of accuracy can be rather limited subject to the availability of a sufficiently representative reduced control space. Another advantage of order-reduction is that it prevents the model from fitting model noise and observational errors [14]. In this study, we follow several previous studies [3, 8, 14, 39] and we use a Proper Orthogonal Decomposition (POD), better known in meteorology and oceanography as Empirical Orthogonal Function (EOF) analysis, to determine the reduced-order control space for our problem.

The reduced-order simulated annealing 4D-VAR approach was implemented in a realistic high resolution setting of the Massachusetts Institute of Technology General Circulation Model (MITgcm) of the tropical Pacific Ocean. This method was used to bring the MITgcm model into more consistency with different real data sets while adjusting the model initial conditions.

---

<sup>†</sup>The PSAS algorithm is equivalent to the indirect representer method [2].

The paper is organized as follows: Section 2 describes the 4D-VAR reduced-order simulated annealing approach. Section 3 presents the implementation of the technique in the MITgcm and analyzes the assimilation results of numerical experiments. Section 4 summarizes and discusses the results of this study.

## 2. THE ASSIMILATION METHOD

### 2.1. The 4D-VAR problem

Assuming that the model physics are accurate, the model state can in principle be brought into agreement, within error estimates, with the observations by adjusting an identifiable set of model parameters. This can be posed as the minimization of a cost function measuring the discrepancy between the model solution and observations over a specified period of time and constrained by the model equations subject to a set of control variables. In its general form, the objective (cost) function consists of a weighted sum of quadratic norms of model-data misfit ( $\mathbf{J}_{obs}$ ) and changes to the control variables ( $\mathbf{J}_c$ ) between the initial time ( $t_0$ ) and the final time ( $t_f$ ) of the assimilation window,

$$\mathbf{J}(\mathbf{c}) = \underbrace{\sum_{t=t_0}^{t_f} [y(t) - H_t(x(t))]^T R_t^{-1} [y(t) - H_t(x(t))]}_{\mathbf{J}_{obs}} + \underbrace{\sum_{t=t_0}^{t_f} [\mathbf{c}(t) - \mathbf{c}^b(t)]^T B_t^{-1} [\mathbf{c}(t) - \mathbf{c}^b(t)]}_{\mathbf{J}_c}, \quad (1)$$

where  $x(t)$  is the model state vector at time  $t$  which evolves in time according to the dynamical model

$$x(t+1) = M_{t+1,t}(x(t)), \quad (2)$$

and  $\mathbf{c}^b(t)$  a first guess (or “background”) representing a priori information about the unknown control vector  $\mathbf{c}(t)$  at time  $t$ .  $\mathbf{c}$  may represent uncertainties in the model parameters, the external forcing fields, and the internal model physics which fully control the evolution of the model state. The vector  $y(t)$  contains all observations available at time  $t$  and is related to the model state according to

$$y(t) = H_t(x(t)) + \varepsilon(t), \quad (3)$$

where  $H_t$  is the observation operator and  $\varepsilon(t)$  represents the associated measurement errors.  $R_t$  and  $B_t$  are weight matrices, usually taken as the inverse of the covariance matrices of the observational and the control (background) uncertainties, respectively. In the formulation of (1), it is implicitly assumed that the errors in the control vector are uncorrelated with the observation errors, and that both errors are mutually uncorrelated in time. This formulation of the 4D-VAR problem is commonly known as the “strong-constraint 4D-VAR” because the model equations are imposed as a strong constraint in the optimization of  $\mathbf{J}$ . The “weak-constraint” formulation allows for a model error (generally additive) in (2), which is then estimated as part of the control vector [2].

In this diagnostic study, as in most 4D-VAR applications, we adjust only the initial conditions  $x_0$  in order to improve the consistency between the model and the data. In this case, the cost function simplifies to

$$\mathbf{J}(\mathbf{X}_0) = \sum_{t=t_0}^{t_f} [y(t) - H_t(x(t))]^T R_t^{-1} [y(t) - H_t(x(t))] + [x_0 - x_0^b]^T B_0^{-1} [x_0 - x_0^b]. \quad (4)$$

The implementation of the approach with more control variables is similar and does not require any noticeable modification, subject to the availability of a reduced-order subspace that sufficiently represents the variability of the control variables [14].

## 2.2. The simulated annealing algorithm

Simulated annealing (SA) is a Monte Carlo sampling technique to find the solution to a global optimization problem by trying random variations of the current solution [18]. It has its origin in the manner in which metals recrystallize in the process of annealing. When a heated metal is cooled very slowly, it freezes at the minimum-energy crystalline structure. Specifically, an SA algorithm moves about randomly looking for a solution in the optimization space that minimizes an objective function, say  $\mathbf{J}$ . A given move may cause  $\mathbf{J}$  to decrease or to increase. Moves that decrease the value of  $\mathbf{J}$  are always accepted. Moves that increase the value of  $\mathbf{J}$  are only accepted with probability  $p = e^{\Delta/T}$ , where  $\Delta$  is the change in the value of  $\mathbf{J}$  and  $T$  is a control parameter called temperature. The allowance for “uphill” moves helps the method to avoid being trapped in a local minima. SA algorithms usually start with large temperature  $T$  to allow uphill moves with large probabilities.  $T$  is then gradually decreased as the search progresses until the probability of accepting a move that increases the objective cost function becomes very unlikely.

Several SA algorithms have been introduced [37, 43]. In the present study, we adopt the SA algorithm proposed by [6], which was successfully tested with various multidimensional optimization problems [12]. In this algorithm, an evaluation of the objective function  $\mathbf{J}$  is first made at the starting point  $\mathbf{c}$  of the control space and its value  $\mathbf{J}(\mathbf{c})$  is recorded. Next, a new control vector  $\mathbf{c}'$  is sampled by varying  $\mathbf{c}$  according to a chosen step length  $v$ ,  $\mathbf{c}' = \mathbf{c} + \theta \cdot v$ , where  $\theta$  is a uniformly distributed random number from  $[-1 \ 1]$ . If  $\mathbf{J}(\mathbf{c}')$  is less than  $\mathbf{J}(\mathbf{c})$ ,  $\mathbf{c}'$  is accepted,  $\mathbf{c}$  is set to  $\mathbf{c}'$ , and the algorithm moves downhill. If  $\mathbf{J}(\mathbf{c}')$  is greater than or equal to  $\mathbf{J}(\mathbf{c})$ ,  $\mathbf{c}'$  is only accepted if  $e^{[(\mathbf{J}(\mathbf{c}')-\mathbf{J}(\mathbf{c}))/T]}$  is greater than a uniformly distributed number from  $[0 \ 1]$ . Periodically, each element of the step length  $v$  is adjusted so that half of all function evaluations in that direction are accepted. A fall in temperature is imposed with an

exponential cooling,  $T_{i+1} = \alpha T_i$ , where  $i$  is the  $i^{\text{th}}$  iteration and  $0 < \alpha < 1$ . As the temperature declines, uphill moves are less likely to be accepted, and the number of rejections rises. As a result, the step lengths decline, given the scheme for their selection. Hence, this SA algorithm focuses upon the most promising area for optimization. The algorithm terminates either when the temperature reaches some final value,  $T_f$ , or when some other stopping criterion has been met.

### *2.3. Order reduction in 4D-VAR*

Simulated annealing provides less sensitivity to nonlinearity than a gradient-based optimization algorithm at the cost of an increase in execution time for a single run of the algorithm [12]. The number of iterations required for the convergence of an SA depends upon the dimension of the optimization problem. In meteorology and oceanography, the dimension of the control vector is of the order of  $10^7 - 10^8$ . The use of SA to solve the 4D-VAR problem seems therefore impractical for these systems.

The physical variables of atmospheric and oceanic models are of high dimension more for numerical accuracy than for physical variability dimensionality. The dissipative and driven nature of these geophysical fluid systems concentrates the energy at large scales, meaning a red spectrum of variability [9], or, for others, suggests the existence of a low-dimensional attractor [24, 34]. In practice, a red spectrum is often indistinguishable from a low-dimensional attractor and both can be efficiently described by a small number of functions (or modes) [32, 46]. In other words, this means that the state of the atmospheric and oceanic models can be accurately modeled in a severely reduced dimensional subspace relative to their phase space. Applying the optimization in a reduced subspace drastically reduces the dimension of the line search of the optimization, which enables the implementation of an SA algorithm

for atmospheric and oceanic 4D-VAR problems. Order reduction enforces a smooth control vector because the line search is only made along some leading modes of the background covariance matrix [24]. Smoothness in the control vector is produced by assuming relatively large spatial scales for the uncertainty of the physical quantity of interest. This means that the cost function will be less irregular in the reduced space with less local minima. This simplifies the optimization problem and increases the likelihood of adjusting the large scale variability of the control vector. Moreover, this attenuates the compensation of model errors into the control adjustments and helps preventing the model from fitting observational noise [14].

Assuming that a set of  $r$  functions  $\mathbf{E} = \{\mathbf{e}_1, \dots, \mathbf{e}_r\}$  describing most of the variability of the control vector of a 4D-VAR problem has been determined, the control vector, of dimension  $n$ , can be represented as

$$\mathbf{c} \approx \sum_{i=1}^r \tilde{c}_i \mathbf{e}_i = \mathbf{E} \tilde{\mathbf{c}}. \quad (5)$$

The idea is then to carry out the optimization with respect to the  $r$  coordinates of the control vector in the reduced-order space  $\tilde{\mathbf{c}} = (\tilde{c}_0, \dots, \tilde{c}_r)$ , rather than the original vector  $\mathbf{c}$ . The dimension of this new control space is therefore equal to the number of functions,  $r$ , retained in (5). In atmospheric and oceanic applications, only a few modes (in the order of 10) are needed to accurately describe most of the variability of interest. Thus the use of an SA algorithm becomes feasible. Starting from a first-guess of the reduced control vector  $\tilde{\mathbf{c}}$ , the full control vector  $\mathbf{c}$  is first recovered using (5). The model (2) is then integrated forward to compute the corresponding cost function  $\mathbf{J}(\tilde{\mathbf{c}})$  as in (1). Following the same steps, another evaluation of the cost function  $\tilde{\mathbf{c}}'$  at an  $r$ -dimension vector  $\tilde{\mathbf{c}}'$  randomly sampled as described in the SA algorithm in section 2.2. If  $\tilde{\mathbf{c}}'$  is accepted by the SA algorithm, then  $\tilde{\mathbf{c}}$  is set to  $\tilde{\mathbf{c}}'$ . If not,  $\tilde{\mathbf{c}}'$  is rejected. The SA is then re-iterated until some stopping criterion is met.

Representing the control vector in a reduced-order subspace implicitly assumes that the

background covariance matrix is of low-rank. This is a straightforward result from (5). Inversely, order-reduction in 4D-VAR can be implemented as well through the use of a low-rank background error covariance matrix  $B_0$  which determines the effective dimension of the minimization problem [4, 10]. This can be easily demonstrated by decomposing the  $n \times n$  background covariance matrix  $B_0$  as  $B_0 = \mathbf{E}\mathbf{E}^T$  and considering the transformation

$$\mathbf{c} = \mathbf{E}\mathbf{d}, \quad (6)$$

where  $\mathbf{E}$  is a  $n \times r$  matrix. The background term of the cost function can simply be written as  $\mathbf{J}_c = \mathbf{d}\mathbf{d}^T$ , which means that the minimization can be conducted with respect to  $\mathbf{d}$  rather than  $\mathbf{c}$ . This further greatly enhances the preconditioning of the optimization problem [7].

The overall performance of a 4D-VAR system greatly depends on the specification of the background error covariance matrix  $B_0$ , as it determines the real dimension of the problem and the importance of the background term  $\mathbf{J}_c$  in the total cost function  $\mathbf{J}$ . It is, however, very difficult to determine an accurate estimate of  $B_0$  because of its huge size and the lack of observations. In the present study, we assume the background covariance matrix of low rank, which is equivalent to parameterizing  $B_0$  in a reduced-order subspace, and the challenge is to determine a good set of basis functions  $\mathbf{E}$ . A good choice of  $\mathbf{E}$  is one that describes most of the variability of the control vector using the minimum number of basis functions. Common techniques are dynamical normal modes or singular vectors [3], empirical modes or EOFs [36], modes based on a series of transformations based on temporal, vertical, and horizontal filters [30]. Fast Fourier and Wavelet transforms are also alternatives for constructing a low-dimensional approximation of the control vector.

In this study, the very popular EOF (or POD) approach has been adopted because it leads to a drastic reduction in the system dimension. This approach has already been successfully used in many previous studies in the context of the adjoint method, e.g. [3, 8, 10, 14, 39].

The EOF analysis is a statistical technique designed to extract the dominant spatial patterns (or gravest modes) of a system that explain the greatest amount of variability from a set of system realizations. These modes are obtained by applying an eigenvalue decomposition to the sample covariance matrix of the system realizations. The dominant modes are those few eigenvectors associated with the largest eigenvalues. An exhaustive discussion of this technique can be found in [36]. Adjusting primarily the control variables in the directions of the gravest modes of the control space, which carry a sizeable amount of the control variance in space and time, is expected to improve the system capability for spreading the information contained in the observations, and therefore to enhance the performance of the optimization procedure.

### 3. NUMERICAL APPLICATION AND RESULTS

#### 3.1. *The ocean model*

To test the reduced-order SA approach for providing a reasonable solution of the 4D-VAR problem, we investigate a realistic eddy-permitting configuration of the MITgcm in the tropical Pacific. The MITgcm is a general circulation model developed at the Massachusetts Institute of Technology (MIT) to support ocean general circulation studies over a broad range of scales and physical processes [28]. It is based on the primitive (Navier-Stokes) equations on a sphere under the Boussinesq approximation. The equations are written in z-coordinates and discretized using the centered second order finite differences approximation in a staggered “Arakawa C-grid”. The MITgcm was used by [42] to produce the first  $2^\circ \times 2^\circ$  global state estimation of the ocean circulation (ECCO).

The regional domain includes the entire tropical Pacific, extending from  $26^\circ\text{S}$  to  $26^\circ\text{N}$  and from  $104^\circ\text{E}$  to  $68^\circ\text{W}$ . The model was set up on a  $1/3^\circ \times 1/3^\circ$  horizontal grid and 39 vertical

levels. The vertical levels are spaced at 10m from the surface to 250m in depth, with spacing gradually increasing to 300m below. The time step is 1 hour. The bathymetry is extracted from the global topography prepared by [40] and adjusted slightly to leave the Indonesian throughflow (ITF) pathways open and to limit the maximum depth to 6000m. The model operated in a hydrostatic mode with an implicit free surface. No-slip conditions are imposed at the lateral boundaries while bottom friction is quadratic with a drag coefficient equal to 0.002. The sub-grid scale physics is a tracer diffusive operator of second order in the vertical, with the eddy coefficients determined by the K-profile parameterization (KPP) model. In the horizontal, diffusive and viscous operators are respectively of second and fourth order with coefficients  $5 \times 10^2 \text{ m}^2/\text{s}$  and  $1 \times 10^{11} \text{ m}^4/\text{s}$ . Vertical diffusivity and viscosity are parameterized by Laplacian mixing with values  $1 \times 10^{-6} \text{ m}^2/\text{s}$  and  $1 \times 10^{-4} \text{ m}^2/\text{s}$ , respectively.

Open boundaries (OB) are set at  $26^\circ\text{S}$  and  $26^\circ\text{N}$ , as well as at four straits in the Indonesian throughflow. The OB are implemented as in [48]. Temperature (T) and salinity (S) and the horizontal components of the velocity (U and V) are specified on the boundary. A smooth transition to the prescribed conditions at the boundaries is achieved by a sponge layer in which the model solution is relaxed to the boundary values. Monthly mean values, extracted from the ECCO global ocean state estimates and centered on the 15th of each month, were prescribed at the grid points just outside the OB and the model solution is relaxed to these values within a buffer zone of  $3^\circ$  over time scales varying linearly from 1 day at the boundary and 40 days at the edge of the zone. The normal velocity fields across the open boundaries have been further adjusted to enforce the same transport at  $26^\circ\text{N}$  and  $26^\circ\text{S}$  as in the global ECCO model, and to exactly balance the volume flux into the domain by the transport out in the ITF.

Atmospheric forcing consists of daily heat and fresh water fluxes, and zonal and meridional

wind stress components extracted from the ECCO global forcing estimates. The ECCO forcings are the NCEP forcings (from the National Centers for Environmental Prediction (NCEP)/National Center for Atmospheric Research (NCAR) re-analysis project [17]), adjusted by a variational  $2^\circ \times 2^\circ$  global state estimation procedure [42]. The ECCO forcings were linearly interpolated over the grid of tropical Pacific model. The model is initialized from rest and Levitus temperature and salinity fields. It is then integrated for a one-month period to geostrophically adjust the velocity fields to the Levitus initial conditions. The model is started from the fields obtained at the end of this one-month integration.

### 3.2. Experiments setup

In this test of the reduced order SA approach, the model was constrained with sea surface height measurements ( $SSH$ ) and  $T$  and  $S$  climatologies over a 4-month period between January and April, 1999.  $SSH$  measurements were provided by the TOPEX/POSEIDON (TP) altimetry mission. To eliminate errors associated with uncertainties in the geoid, the mean  $\overline{SSH}$  and time-varying  $SSH'$  components of the  $SSH$  data were considered separately. The mapped 1999 TP mean  $SSH$  minus the Earth Gravitational Model 1996 (EGM96) geoid [23] has been used to constrain the mean model  $SSH$  during the assimilation. For the time-varying component, along-track daily TP data obtained from NASA's PO-DAAC at JPL and processed as described by [41] were fit at the observation points. Although ocean climatologies are not usually considered "observations", they provide a pre-smoothed analysis of observations and they can be used to constrain the model solution. Here, the Levitus climatology of monthly mean  $T$  and  $S$  [25], and the Reynolds monthly sea surface temperature ( $SST$ ) [38] were used. The Levitus climatology is based on historical hydrographic data that are merged and spatially averaged. The Reynolds optimum interpolation (OI)  $SST$  analyses are produced on a

one-degree grid using buoy and ship data as well as satellite *SST* data. These “data” sets were interpolated onto the model grid first horizontally and then vertically using linear interpolation procedures.

The control vector consists of the model initial salinity  $S_0$ , temperature  $T_0$ , horizontal velocities  $U_0$  and  $V_0$ , and sea surface height  $SSH_0$ . The explicit form of the the cost function is then

$$\begin{aligned}
\mathbf{J} = & \left[ \overline{SSH} - \overline{SSH}_{TP-EGM96} \right]^T \mathbf{R}_{TP-EGM96}^{-1} \left[ \overline{SSH} - \overline{SSH}_{TP-EGM96} \right] \\
& + \sum_{t=days} \left[ SSH'(t) - SSH'_{TP}(t) \right]^T \mathbf{R}_{TP}^{-1} \left[ SSH'(t) - SSH'_{TP}(t) \right] \\
& + \sum_{t=months} \left[ SST(t) - SST_{Reynolds}(t) \right]^T \mathbf{R}_{Reynolds}^{-1} \left[ SST(t) - SST_{Reynolds}(t) \right] \\
& + \sum_{t=months} \left[ T(t) - T_{Levitus}(t) \right]^T \mathbf{R}_{T_{Levitus}}^{-1} \left[ T(t) - T_{Levitus}(t) \right] \\
& + \sum_{t=months} \left[ S(t) - S_{Levitus}(t) \right]^T \mathbf{R}_{S_{Levitus}}^{-1} \left[ S(t) - S_{Levitus}(t) \right] \\
& + \left[ S_0 - S_0^b \right]^T B_{S_0}^{-1} \left[ S_0 - S_0^b \right] + \left[ T_0 - T_0^b \right]^T B_{T_0}^{-1} \left[ T_0 - T_0^b \right] \\
& + \left[ U_0 - U_0^b \right]^T B_{U_0}^{-1} \left[ U_0 - U_0^b \right] + \left[ V_0 - V_0^b \right]^T B_{V_0}^{-1} \left[ V_0 - V_0^b \right] \\
& + \left[ SSH_0 - SSH_0^b \right]^T B_{SSH_0}^{-1} \left[ SSH_0 - SSH_0^b \right]^T.
\end{aligned}$$

In this preliminary study, as in most applications, measurement errors were assumed to be spatially uncorrelated. Errors in the data are then only prescribed along the diagonal of the error covariances. They have been approximated by the error profiles for temperature and salinity taken from Levitus data and by 50% of the data variability for the *SSH*. As stated in section 2.3, the background covariance matrix is parametrized via a set of few EOFs. The EOFs need to be carefully chosen in order to efficiently represent the variability of the control vector. The choice of the sample of realizations from which the EOFs are computed is therefore key for building an efficient reduced-order 4D-VAR system. In our case, the model initial conditions are control variables and the EOFs could be computed from a time series of

system state vectors, assuming that the structure of the initial conditions errors is correlated with the variances of the system state. Since a sample of “true” system realizations is not available in practice, we follow the common strategy of [34] and we compute the EOFs from a set of model outputs. Of course, the resulting subspace will not cover all the variability of the control variables. This means that some of the variability of the initial conditions will be in the null space, and will therefore not be explored by the optimization algorithm. This is, however, not a serious handicap for the present study, as we aim at demonstrating the possibility of using an SA algorithm to determine a reasonable solution for a highly nonlinear 4D-VAR problem. As will be shown below, this restricted subspace search will lead to a satisfactory reduction in the cost function in our experiments. Another benefit from computing the EOFs from a sample of model realizations is that these functions will respect the dynamics of the model, and will therefore improve the consistency between the adjusted initial conditions and the model dynamics. This set of EOFs can always be enhanced in the future by adding realizations of optimized model outputs as suggested by [14].

To sample realizations of model outputs, the model was first integrated for 2-year period between January 1997 and December 1998 to achieve a quasi-adjustment of the model dynamics to the NCEP interannual forcing. Next, another integration of one year, beginning January 1999 was carried out to generate a ‘historical’ sequence of model outputs sampled every 3 days. Since the variables needed to initialize the ocean model have different units, a multivariate EOF analysis was applied on the 120 retained model state vectors. In this analysis, all model variables were normalized by the square-root of their variances spatially averaged over all model sea grid points. Figure 1 plots the fraction of the variance (often called inertia) captured by the EOFs as a function of the dimension of the reduced space (number of retained EOFs). Clearly, the first EOFs capture most of the variability of the

model realizations, suggesting that only a few EOFs are needed to represent most of the variability of the system. In the following, we retained 10 EOFs which account for almost 95% of the system total variance. The optimization was then performed in a subspace of dimension 10 rather than 8,975,170.

In order to apply the SA algorithm described in section 2.2 to a specific problem, one must specify the state space, the neighbor selection method, the probability transition function, and the annealing schedule. These choices can have a significant impact on the method's effectiveness. Inappropriate choice of the parameters may cause the solution to be trapped at one of the local minima. Since it is practically impossible to theoretically set the parameters of the SA algorithm, several experiments were performed with varieties of values to empirically determine an acceptable set of parameters. We present here the one experiment that shows the model fit in the best light, in term of overall decrease in the total cost function. Readers are referred to the in-depth review of [12] for detailed discussion on the variables used in this algorithm. The values of the variables intrinsic to the algorithm that were used in these analyses were: initial step length  $v = 2$ , initial temperature  $T_0 = 2.5 * 10^5$ , rate of temperature change  $\alpha$  is 0.5. Maximum number of iterations was set to 500. The background state was taken as the starting point for minimization, which means that the background term  $\mathbf{J}_c$  in the cost function is zero at the initial time.

### 3.3. Numerical results

Results of assimilation experiments are now presented. We note that under the same setup, the optimization of the total cost function using the “full” adjoint method and a quasi-newton optimization algorithm was not successful because of exponentially increasing adjoint sensitivities that appeared after 2-3 months integration of the adjoint model [15].

The evolution of the total cost function  $\mathbf{J}$  as a function of the number of optimization steps (number of model integrations) is plotted in Figure 2. Accepted steps are indicated by circles. Overall, the total cost function decreased by about 60% after 150 optimization steps. This is a significant improvement in the model/data consistency, given the strongly nonlinear character of the cost function that prevented any improvement with the classical adjoint method. A total of 150 iterations with the SA algorithm is comparable to 30 iterations with the adjoint method, as one single iteration of the adjoint model requires about 5 times the CPU time of a forward model run. More specifically, a total number of 72 2.8GHZ PIV-Xeon processors were used with a wall clock of approximately 52 minutes and a total memory cost of about 9.8G for a forward run and 212 minutes and 37.8G for a backward adjoint model run. For this particular 4D-VAR problem, this means that one iteration with adjoint method is equivalent to about 5 (1 forward plus 4 backward run) times the CPU time and 4 times the memory cost needed for one iteration with the SA algorithm. The decrease in the total cost function is shown to be fast at the early optimization iterations and seems to stagnate after the 370<sup>th</sup> step. This is similar to the results usually obtained with an adjoint-based 4D-VAR in which the most significant cost function decrease is attained by the early optimization steps. It is also in line with the character of the optimization reduced subspace that explains the energetic variability of the system. After 500 iterations, the SA algorithm did not converge and was stopped because the maximum number of steps had been reached. Several uphill moves ( $\sim 55\%$  of the total number of steps) were randomly accepted, which might have helped the algorithm escaping local minima. As can be seen in Figure 2, steps that led to a large increase in the cost function were often discarded because of the rather conservative value of the initial temperature  $T_0$ , which means faster convergence rate of the optimization at the risk of being trapped in a local manifold. This choice of  $T_0$  was adopted in order to obtain an acceptable decrease of the cost

function at an affordable number of cost function evaluations, as we only aim to show that the use of an SA algorithm would enable the optimization of a strongly nonlinear 4D-VAR problem.

The final decrease for each individual contribution of the model/data differences in the total cost function, including full depth  $T$ ,  $S$ ,  $SST$ , and  $SSH$  is shown in Figure 3. Cost terms were normalized by the number of observations in the sum over time and/or space, so a value of 1 would roughly indicate that the solution fits the data within the specified uncertainties. The overall improvement is found to be different for each model state variable. More precisely, the assimilation enhanced the model fit to the data by almost 65% with the Levitus  $T$  and  $S$  climatology, 50% with the Reynolds  $SST$  reanalysis, and 36% and 3% respectively with the TOPEX mean and anomalies  $SSH$  data. Quite clearly, the most significant improvement was obtained for the temperature and salinity fields. This is probably because the controllability of  $S$  and  $T$  is quite efficient with the model initial conditions even over relatively long assimilation periods. This is particularly true in the deep ocean where the variability of these fields is rather weak. The large misfit measuring the deviations of the model  $T$  and  $S$  from the Levitus data sets is another reason behind the good performance of the assimilation system with these variables. Accordingly, the optimization worked on removing those large misfits during the first iterations. The fit to the  $SST$  field is less important but still consequent. Concerning the  $SSH$  field, the assimilation reduced the model discrepancy with the mean TOPEX  $SSH$  field. However, it was not able to significantly improve the fit of the model  $SSH$  field to the TOPEX anomalies data. The restrained controllability of the  $SSH$  anomaly field by the model initial conditions is probably one of the reasons behind this limited performance with  $SSH$ . The “smoothed” large-scale character and the small number of degrees of freedom of the EOF subspace might have also restricted the line search for the solution, thus restricting

the model fit to the small-scale variability observed in the TOPEX *SSH* anomalies. The use of more EOFs only marginally improved the assimilation results for this variable in the present setup while significantly slowing the convergence rate of the optimization. This is because the last EOFs are often contaminated with spurious correlations which might even degrade the representativeness of the reduced control space [13]. In summary, the assimilation was able to improve the model fit to the data within the specified observational errors except for the TOPEX *SSH* anomalies measurements. Increasing the contribution of the *SSH* term in the total cost function by directly attributing larger weights to these measurements or indirectly through the assimilation of in-situ subsurface *S* and *T* data that is in balance with altimetry would force the optimization algorithm to focus more on this term. The use of time-varying forcing fields as control variables would provide more controllability of the model *SSH* allowing better fit to the assimilated TOPEX *SSH* measurements [15].

The monthly-averaged normalized cost function for *SST* plotted in Figure 4 is small in January, as the assimilation starts from field close to the Levitus data, and then increases over time as the model drifts from Reynolds *SST*. The assimilation efficiently reduces the drift and brings the model close to the observations over the 4-month assimilation period. The fit to the data in the last two months is not as good as in the first two months. The spatial contribution to the cost function summed over the entire interval is shown for the salinity term in Figure 5. The misfits were normalized by the misfits from the reference run (without assimilation), so a value of 1 would indicate that the assimilation improves the fit to the data. It can be seen that the model/data misfit is reduced over the entire domain. Normalized misfit variance is higher near Indonesia, although it is less than 1. This is probably due to complicated topographic interactions in the region, the slow adjustment of salinity in the west, and from anomalies in the climatology fields near the coast.

Histograms of the model/data misfits (residuals) are shown in Figure 6 from the reference run and the assimilation run for Reynolds *SST* and Levitus salinity. For the reference run, the mean and standard deviation of the residuals are  $0.3^{\circ}C$  and  $0.38^{\circ}C$  for Reynolds data and  $0.21PSU$  and  $0.3PSU$  for Levitus data. The statistics of the residual are improved by the assimilation with smaller means  $0.23^{\circ}C$  and  $0.12PSU$ , and more compact standard deviations  $0.3^{\circ}C$  and  $0.21PSU$  for Reynolds *SST* and Levitus salinity, respectively. Moreover, the distribution of the assimilated residuals fits a normal distribution better, suggesting that this ‘least-squares’ fit is close to being the estimator of maximum likelihood.

Finally, to assess the fit to the assimilated observations in a more physical way, we compared a zonal cross-section of the mean temperature field at the equator from the reference and the assimilation runs to the Levitus field (left panel of Figure 7). The thermocline from the reference run is shallower than in the data in the western part of the Pacific and deeper in the eastern part. The thermocline tilt (and the Equatorial Undercurrent (EUC) that moves along it) are thought to be strongly influenced by the wind stress [29]. The assimilation improves the tilt of the thermocline and enhances the agreement of the temperature field with climatology, even in the deep layers. This is to be expected from the reduction in the temperature errors seen in the cost function, since these are not independent measurements.

#### 4. DISCUSSION

Four-dimensional variational (4D-VAR) assimilation problems are generally solved using an adjoint-based optimization algorithm. Such techniques are popular because of their fast convergence rate toward the minimum, when properly preconditioned, and because of the efficiency of the adjoint method for determining the gradients of the cost function of the 4D-VAR problem with respect to the control variables. The adjoint model provides the gradients

at the expense of few model integrations (about 5 in the present system). Recent studies have seriously questioned the applicability of the adjoint method to assimilate data over long periods with state-of-the-art strongly nonlinear atmospheric and oceanic models. In such systems, the cost function becomes far too irregular to be optimized with a gradient-based optimization algorithm since these algorithms are only designed to converge toward local minima.

In this study, a simulated annealing (SA) technique was used to search for the minimum of the cost function of a strongly nonlinear 4D-VAR ocean problem. SA is a Monte-Carlo global optimization method that stochastically explores the search space looking for the optimum of the cost function. Manifold changes to escape local minima are allowed with a probability that gradually decreases in the manner in which metals recrystallize in the process of annealing. Exploring the search space may however require a prohibitive number of model integrations in modern atmospheric and oceanic applications given the huge dimension of their control vectors. An order-reduction was then used to reduce the dimension of the control space. It is well-known that order-reduction generally leads to a drastic reduction in the dimension of atmospheric and oceanic variables because of the red spectrum that governs the variability of these systems. Here, the reduced-order control space was determined via a set of empirical orthogonal functions (EOFs). The EOFs were computed from a historical set of model outputs, as the control vector in our application consisted of the initial conditions of the model.

The reduced-order SA approach was implemented to constrain an eddy-permitting primitive equation ocean model of the tropical Pacific Ocean with climatology and satellite altimetry data. In this same setup, the adjoint method failed to make any significant improvement in the model/data consistency over long assimilation windows (longer than 4 months for the present system) because of the appearance of exponentially increasing sensitivities in the adjoint model after only 2 – 3 months integrations. Such sensitivities were associated with the existence of

a large number of tightly packed local minima in the cost function of this strongly nonlinear 4D-VAR problem. Numerical experiments presented in this paper demonstrated the capability of the reduced-order SA approach in reducing the cost function while efficiently escaping from local minima. The overall total improvement of the model/data consistency was more than 50% after less than 150 optimization steps (model integrations). In terms of computational cost, this is comparable to 30 iterations with the adjoint method in our system. Concentrating the variability of the system in a few EOFs enhanced the system capability for spreading the information contained in the observations, and certainly helped improving the convergence rate of the SA algorithm. The use of EOFs was also found to be beneficial in preventing the model from fitting model noise and observational errors. The method failed, however, to significantly improve the model *SSH* fit with TOPEX altimetry anomalies. This poor performance was attributed to the weak controllability of the *SSH* field by the initial conditions, and by the limited number of degrees of freedom of the line search that prevented the model from fitting eddy variability observed in the *SSH* measurements.

The efficiency of the reduced-order SA approach depends on two factors: the quality of the reduced space, and the available computing resources. The performance of the system will always be limited by the representativeness and the restricted number of degrees of freedom of the prior estimate of the control subspace. Using localization techniques of the control subspace (analogously to subspace Kalman filters) would enhance the performance of the method, but may result in an increase of the dimension of the search space. The convergence of the SA algorithm can be difficult to reach given the restricted number of model integrations that can be performed. This means that the solution obtained with this approach might not be optimal, even in the reduced space. Reaching optimality is however an over-optimistic goal and is never guaranteed, especially when the optimization is applied in the full control space.

Our poor knowledge of the error covariance matrices also suggests that optimality is relative to our estimates of these matrices. One should rather seek a satisfactory dynamical solution that sufficiently fits the data. Having this goal in mind, a reduced-order SA algorithm appears as a plausible approach to solve a strongly nonlinear 4D-VAR assimilation problem; it is easy to implement and does not require the complex development of the adjoint model. This approach provided acceptable results in the present study, and was able to improve the model/data consistency when the adjoint method completely failed under the same setup. It was also capable to escape the numerous local minima of this strongly nonlinear optimization problem and provided a satisfactory solution with an affordable number of model integrations. Several studies have suggested that the adjoint method might work if the first-guess is close enough to the minimum, assuming that the cost function is convex in the manifold of the minimum. Another possible application of the reduced-order SA approach would be to first use it in order to find the manifold of the minimum and then continue the optimization with the full adjoint method to sharpen the minimum achieved via SA as suggested by [31]. This study demonstrated that an SA can be used in the context of a particular high dimensional 4D-VAR problem. Further studies need to be conducted with different and further complex setups, e.g. higher resolution models and assimilation of more multivariate data sets, for more evaluation of the efficiency of the method and for better understanding of its performance.

## REFERENCES

1. Barth N, Wunsch C. Oceanographic experiment design by simulated annealing. *Journal of Physical Oceanography* 1990; **20**: 1249-1263.
2. Bennett A. *Inverse methods in physical oceanography*. Cambridge University Press, 256 pp., 2002.
3. Blayo E, Durbiano S, Vidard PA, Le Dimet FX. Reduced order strategies for variational data assimilation

- in oceanic models. *In Data Assimilation for Geophysical Flows*, B. Sportisse, F.-X. Le Dimet (eds.), Springer-Verlag, 2003.
4. Bonekamp H, Van Oldenborgh GJ, Burgers G. Variational assimilation of TAO and XBT data in the HOPE OGCM, adjusting the surface fluxes in the tropical ocean. *Journal of Geophysical Research* 1991; **106**: 16693-16709.
  5. Cao Y, Zhu J, Navon IM, Luo Z. A reduced-order approach to four-dimensional variational data assimilation using proper orthogonal decomposition. *International Journal for Numerical Methods in Fluids* 2007; **53**: 1571-158.
  6. Corana A, Marchesi M, Martini C, Ridella S. Minimizing multimodal functions of continuous variables with the simulated annealing algorithm. *ACM Transactions on Mathematical Software*; **13**: 262-280.
  7. Courtier P, Thépaut JN, Hollingsworth A. A strategy for operational implementation of 4D-Var, using an incremental approach. *Quarterly Journal of Royal Meteorological Society* 1994; **120**: 1367-1387.
  8. Daescu DN, Navon IM. Efficiency of a POD-based reduced second-order adjoint model in 4D-Var data assimilation. *International Journal for Numerical Methods in Fluids* 2007; **53**: 985-1004.
  9. Daley R, Barker E. NAVDAS: Formulation and Diagnostics. *Monthly Weather Review* 2000; **129**: 869-883.
  10. Fujii Y, Kamachi M. A Reconstruction of Observed Profiles in the Sea East of Japan Using Vertical Coupled Temperature-Salinity EOF Modes. *Journal of Oceanography* 2003; **59**: 173-186.
  11. Ghil M, Malanotte-Rizzoli P. Data assimilation in meteorology and oceanography. *Advances in Geophysics* 1991; **33**: 141-266.
  12. Goffe WL, Ferrier GD, Rogers J. Global optimization of statistical functions with simulated annealing. *Journal of Econometrics* 1994; **60**: 65-99.
  13. Hoteit I, Pham DT, Blum J. A semi-evolutive Kalman filter with partially local correction basis for data assimilation in oceanography. *Oceanologica Acta* 2003; **26**, 511-524.
  14. Hoteit I, Köhl A. Efficiency of reduced-order, time-dependent adjoint data assimilation approaches *Journal of Oceanography* 2006; **62**(4): 539-550.
  15. Hoteit I, Cornuelle B, Köhl A, Stammer D. Treating strong adjoint sensitivities in tropical eddy-permitting variational data assimilation. *Quarterly Journal of Royal Meteorological Society* 2006; **123**: 2449-2461.
  16. Hurtt GC, Armstrong RA. A pelagic ecosystem model calibrated with BATS data. *Deep-Sea Research* 1996; **43**: 653-683.
  17. Kalnay E, and coauthors. The NCEP/NCAR re-analysis project. *Bulletin of the American Meteorological Society* 1996; **77**: 437-471.
  18. Kirkpatrick A, Gelatt CD, Vecchi MP. Optimization by Simulated Annealing. *Science* 1983; **220**: 671-680.

19. Köhl A, Willebrand J. An adjoint method for the assimilation of statistical characteristics into eddy-resolving ocean models. *Tellus* 2002; **54**: 406-425.
20. Kruger J. Simulated annealing: A tool for data assimilation into an almost steady model state. *Journal of Physical Oceanography* 1993; **23**: 679-688.
21. Lea DJ, Haine TWN, Allen MR, Hansen JA. Sensitivity analysis of the climate of a chaotic ocean circulation model. *Quarterly Journal of Royal Meteorological Society* 2002; **128**: 2587-2606.
22. Le Dimet FX, Talagrand O. Variational algorithms for analysis and assimilation of meteorological observations. Theoretical aspects. *Tellus* 1986; **38**: 97-110.
23. Lemoine F, and coauthors. The development of the NASA GSFC and NIMA joint geopotential model. *International Association of Geodesy Symposium* 1996; Tokyo, Japan, **117**: 461-469.
24. Lermusiaux PFJ, Robinson A. Data Assimilation via Error Subspace Statistical Estimation, Part I: Theory and Schemes. *Monthly Weather Review* 1999; **127**: 1385-1407.
25. Levitus S, Boyer TP. World Ocean atlas 1994. *NOAA atlas NESDIS*, 1994; **3-4**, US Govt Printing Office, Washington, DC.
26. Li Y. A note on the uniqueness problem of variational adjustment approach to four-dimensional data assimilation. *Journal of Meteorological Society Japan* 1991; **69**: 581-585.
27. Matear R.J. Parameter optimization and analysis of ecosystem models using simulated annealing: A case study at Station P. *Journal of Marine Research* 2000; **53**(4): 571-607.
28. Marshall J, Adcroft A, Hill C, Perelman L, Heisey C. A finite-volume, incompressible Navier Stokes model for studies of the ocean on parallel computers. *Journal of Geophysical Research* 1997; **102**: 5753-5766.
29. McCreary JP, Lu P. Interaction between the Subtropical and Equatorial Ocean Circulations: The Subtropical Cell. *Journal of Physical Oceanography* 1994; **24**: 466-497.
30. Menemenlis D, Wunsch C. Linearization of an oceanic general circulation model for data assimilation and climate studies. *Journal of Atmospheric and Oceanic Technology* 1997; **14**: 1420-1443.
31. Navon IM, Brown F, and Robertson DH. Combined Simulated-Annealing and Limited-Memory Quasi-Newton Methods for Determining Structure of Mixed Argon-Xenon Molecular Clusters, *Computers and Chemistry* 1990, **14**: 305-3.
32. Osborne AR, Pastorello A. Simultaneous occurrence of low-dimensional chaos and colored random noise in nonlinear physical systems. *Physics letters. A* 1993; **181**: 159-171.
33. Pathmathevan M, Koike T, Li X. A new satellite-based data assimilation algorithm to determine spatial and temporal variations of soil moisture and temperature profiles. *Journal of the Meteorological Society of Japan* 2003; **81**: 1111-1135.

34. Pham DT, Verron J, Roubaud MC. Singular evolutive Kalman filter with EOF initialization for data assimilation in oceanography. *Journal Marine Systems* 1997; **16**: 323-340.
35. Pires C, Vautard R, Talagrand O. On extending the limits of variational assimilation in nonlinear chaotic systems. *Tellus* 1996; **48**: 96-121.
36. Preisendorfer R. *Principal component analysis in meteorology and oceanography*. Elsevier, 1988.
37. Press WH, Flannery BP, Teukolsky SA, Vetterling WT. *Fortran Numerical Recipes, Vol. 1, Numerical Recipes in Fortran 77: The Art of Scientific Computing*. Cambridge University Press, New York, 1996.
38. Reynolds RW, Smith TM. Improved global sea surface temperature analysis using optimum interpolation. *Journal of Climate* 1994; **7**: 929-948.
39. Robert C, Durbiano S, Blayo E, Verron J, Blum J, Le Dimet FX. A reduced-order strategy for 4D-Var data assimilation. *Journal of Marine Systems* 2005; **57**: 70-82
40. Smith W, Sandwell D. Global seafloor topography from satellite altimetry and ship depth soundings. *Science* 1997; **277**: 1956-1962.
41. Stammer D, Wunsch C. Preliminary assessment of the accuracy and precision of TOPEX/POSEIDON altimeter data with respect to the large scale ocean circulation. *Journal of Geophysical Research* 1994; **99**: 24584-24604.
42. Stammer D, Wunsch C, Giering R, Eckert C, Heimbach P, Marotzke J, Adcroft A, Hill CN, Marshall J. The global ocean circulation during 1992-1997, estimated from ocean observations and a general circulation model. *Journal of Geophysical Research* 2002; **107**(C9): 3118.
43. Van Laarhoven PJM, Aarts EHL. *Simulated annealing: theory and applications*. D. Reidel Publishing Company, The Netherlands, 1987.
44. Vallino JJ. Improving marine ecosystem models: use of data assimilation and mesocosm experiments. *Journal of Marine Research* 2000; **58**(1): 117-164.
45. Vidard PA, Blayo E, Le Dimet FX. 4D variational data analysis with imperfect model. *Flow, Turbulence and Combustion* 2000; **65**: 489-504.
46. West BJ, Mackey HJ. Geophysical attractors may be only colored noise *Journal of Applied Physics* 1991; **69**: 6747-6749.
47. Wunsch C. *The ocean circulation inverse problem*. Cambridge University Press, New York, 1996.
48. Zhang KQ, Marotzke J. The importance of open boundary estimation for an Indian ocean GCM data synthesis. *Journal of Marine Research* 2002; **57**: 305-334.
49. Zhu J, Kamachi M, Hui W. The improvement made by a modified TLM in 4DVAR with a geophysical boundary layer model. *Advances in Atmospheric Sciences* 2002; **19**: 563-582.

List of Figures

1	Fraction of the variance (inertia) captured by the EOFs . . . . .	30
2	Decrease of the total cost function with the number of iterations . . . . .	31
3	Diagram of individual contributions of data cost function terms . . . . .	32
4	Evolution in time of the normalized cost contribution from the <i>SST</i> misfit . . . . .	33
5	Spatial distribution of the cost contribution from the Levitus salinity misfit . . . . .	34
6	Histograms of model/data misfits . . . . .	35
7	Zonal cross-sections along the equator of the mean temperature . . . . .	36

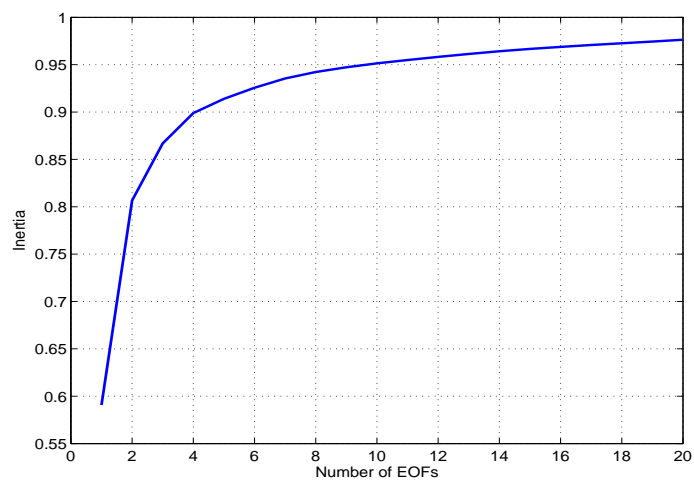


Figure 1. Fraction of the variance (inertia) captured by the EOFs as a function of the number of EOFs.

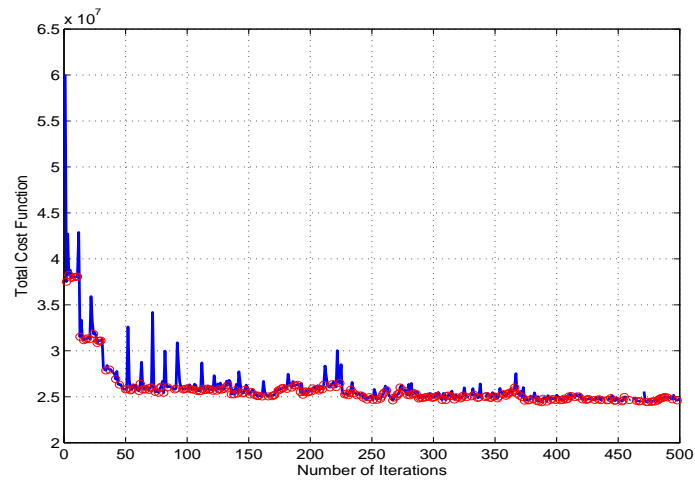


Figure 2. Decrease of the total cost function with the number of iterations. Circles indicate accepted iterations.

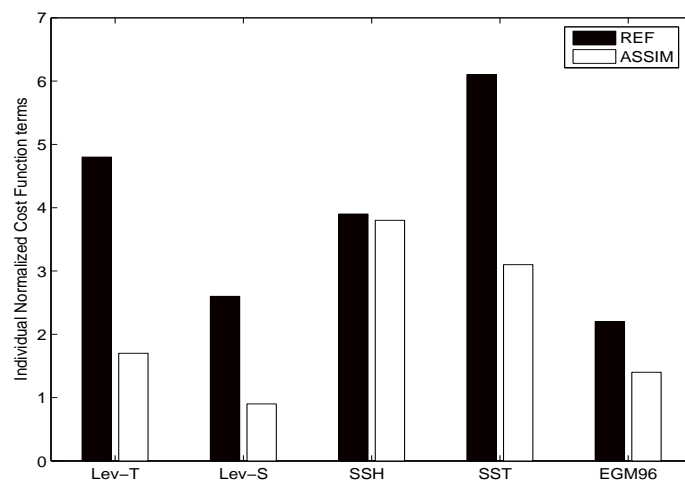


Figure 3. Diagram of individual contributions of the data cost function terms comparing the cost values from the reference run and from the assimilation run.

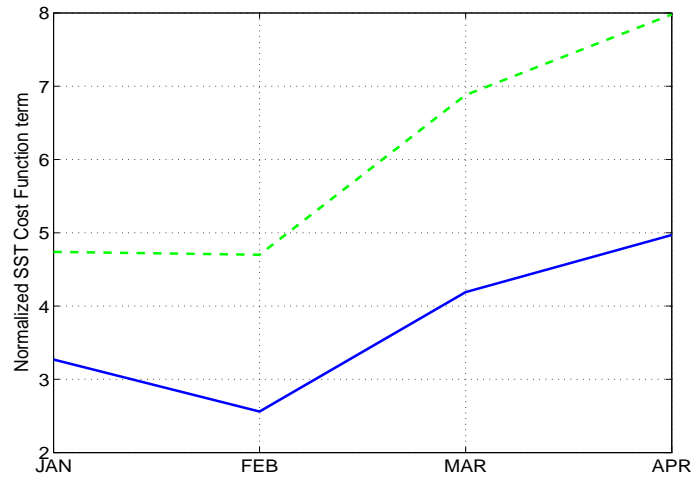


Figure 4. Evolution in time of the normalized cost contribution from the Reynolds *SST* misfit (summed month by month) from the reference run (dashed curve) and the assimilation run (solid curve).

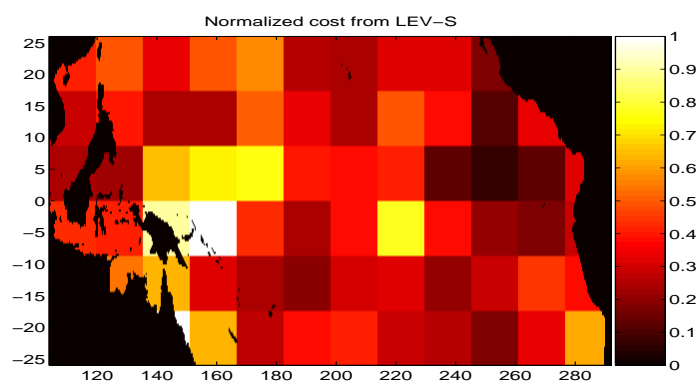


Figure 5. Fraction between the spatial distributions of the cost contribution for the Levitus salinity misfit averaged over  $25^\circ \times 8^\circ$  boxes before (reference) and after assimilation.

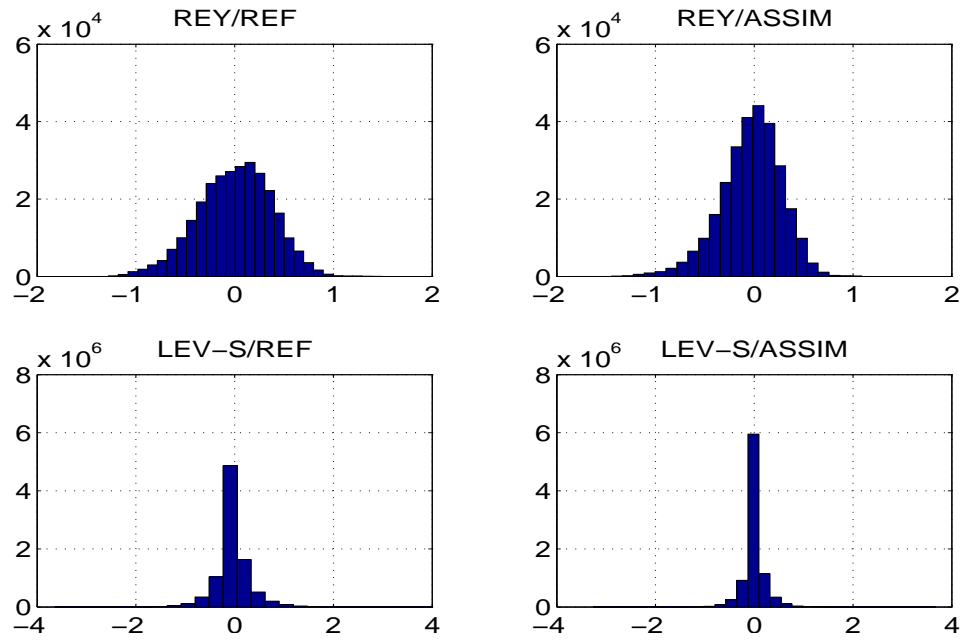


Figure 6. Histogram of model/data misfits (residuals) from the reference run (left) and the assimilation run (right) for Reynolds *SST* (top) and Levitus salinity (bottom).

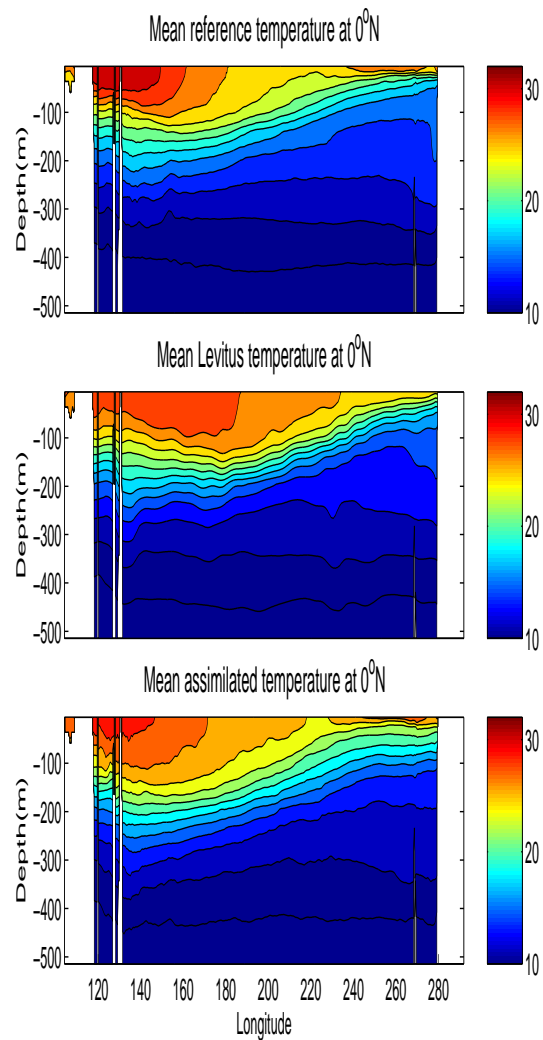


Figure 7. *Left column:* Zonal cross-sections along the equator of the mean temperature ( $^{\circ}\text{C}$ ) averaged over the assimilation period from the reference run (top panel), from Levitus (middle panel), and from the assimilation run (bottom panel).